JOURNAL OF MATERIALS SCIENCE 31 (1996) 4181–4187

Dynamic analysis of fibre breakage in single- and multiple-fibre composites

M.L. ACCORSI, A. PEGORETTI*‡, A.T. DIBENEDETTO‡
Department of Civil Engineering, and ‡Department of Chemical Engineering and Institute of Materials Science, University of Connecticut, Storrs, CT 06269, USA

The dynamic effects associated with fibre breakage in single- and multiple-fibre composites were investigated using the finite element method. The goal of this work was to determine if the dynamic stresses differed significantly from the static stresses and, consequently, if dynamic effects were important in the prediction of subsequent fracture of the composite. For single-fibre composites, dynamic and static analyses were performed over a range of modulus values for epoxy matrices with a glass fibre to establish a range of the dynamic effects. The maximum dynamic stresses, spatial distribution of dynamic stresses, and corresponding times were evaluated. For multiple-fibre composites, the dynamic effects associated with single- and double-fibre breakage were investigated for a typical epoxy/glass composite and compared to the corresponding static problems.

1. Introduction

In continuous fibre-reinforced composites, individual fibre filaments can fracture at stresses less than 50% of the ultimate strength of the composite. As the stress increases, fibre filaments continue to break at locations throughout the material until enough breaks occur cumulatively at one location to produce a defect large enough to cause catastrophic failure. Variation in filament strengths tends to offset the effects of stress concentrations at fibre breaks, thus favouring random fibre fracture rather than cumulative ones at the site of an initial fracture (i.e. co-ordinated fibre fracture). It has been found experimentally, however, that a co-ordinated number of fibre fractures can occur at interfibre spacings of up to approximately six to eight fibre diameters, with strong co-ordination at interfibre spacings less than four [1, 2]. Such patterns appear to be dependent on the fibre volume fraction and the nature of the localized matrix fracture and interface debonding at the site of the filament fracture.

At the instant a continuous filament is fractured, the broken fibre end loses load and retracts in the matrix. A compressive stress wave moves through the fibre and a multiaxial stress wave moves out into the matrix, creating a significant overshooting of the equilibrium stresses at the filament fracture site. The stored energy lost in the region around the fibre end generates fractures in the matrix and/or along the interface as well as localized stress concentrations in adjacent fibres. In a recent study, a linear finite element method (LFEM) has been used to calculate the initiation and arrest strain energy release rates for these different modes of propagation [3]. For an S-glass fibre/epoxy matrix microcomposite with the same constituent properties as used in this study, strain energy release rates in the range of 130–340 $J m^{-2}$ for interface debonding and 80–100 $J m^{-2}$ for matrix cracking were obtained. In another study [4], it was shown that the static equilibrium stresses in adjacent fibres, generated by the fracture of a single filament, significantly increased the probability of a co-ordinated pattern of sequential fibre fractures. An LFEM analysis was used to simulate the fracture of a single filament in a continuous E-glass fibre-reinforced epoxy composite. It was shown that at constant strain, subsequent failure of the adjacent fibre is constrained to within about three to five fibre diameters distance from the broken end [4]. The computer simulations showed that even under static conditions, the probability of subsequent failure of an adjacent filament could attain levels of the order of 30%–40% at a stress equal to the average breaking strength of a single filament. Experimentally, it was observed that in E-glass/epoxy multiple fibre microcomposites the subsequent failures occurred instantaneously, thus suggesting that dynamic processes were operative. Preliminary LFEM simulations showed that the dynamic stress waves generated at the instant of filament fracture caused significant overshooting of the equilibrium stress concentration factors in the adjacent fibres. Because the probability of failure of a glass fibre depends exponentially on the level of stress, it is apparent that the nature of the dynamic stress waves could have a significant effect on co-ordinated patterns of fibre fracture and, thus, on the generation of critical defects in continuous fibre-reinforced composites.

In this study, we used the MARC finite element code to examine the dynamic stress patterns generated

Permanent address: Department of Materials Engineering, University of Trento, via Mesiano 77, 38050 Trento, Italy.

0022–2461

within the first 100 ns of a fracture event in both single and multiple glass fibre microcomposites. It was shown that the dynamic stress waves have a significant effect on the probability of localized failure of adjacent fibres in the region of the initial fracture site.

2. Single-fibre composite

In this section, the dynamic effects associated with a fibre break in a single-fibre composite are investigated. The model considered consists of an infinite epoxy matrix containing a single glass fibre, as shown in Fig. 1a. An axisymmetric finite element (FE) model of plane ABCDEF, as shown in Fig. 1b, is used for the analysis. The dimensions of the FE model are chosen large enough so that the waves produced by fibre breakage do not impinge upon the boundaries during the time period considered. These dimensions are dependent upon the wave speeds in the fibre and matrix. For the materials considered, values of $d_r = 55\ \mu m$ and $d_z = 300\ \mu m$ were used. Approximately 2600 axisymmetric solid elements were used in the FE model.

It is desired to load the FE model quasi-statically up to fibre breakage, then introduce a break in the fibre along edge BC. Because this problem is linear, it is sufficient to break the fibre at 1% strain and scale these results by the actual fibre breakage strain. Appropriate boundary conditions are required along the four edges of the FE model to simulate the problem. Edge AD is a free edge. As previously mentioned, d_r is chosen sufficiently large so that the stresses along AD correspond to uniform stresses in an infinite matrix material. Along edge CF, the radial displacement is prescribed to be zero. A uniform displacement in the z direction is prescribed along edge DEF. To simulate the experimental procedure, the displacement is increased quasi-statically up to fibre breakage, then held constant. Prior to fibre breakage, the displacement in the z direction along edge ABC is zero. At fibre breakage, this displacement boundary condition is released along edge BC and retained along edge AB.

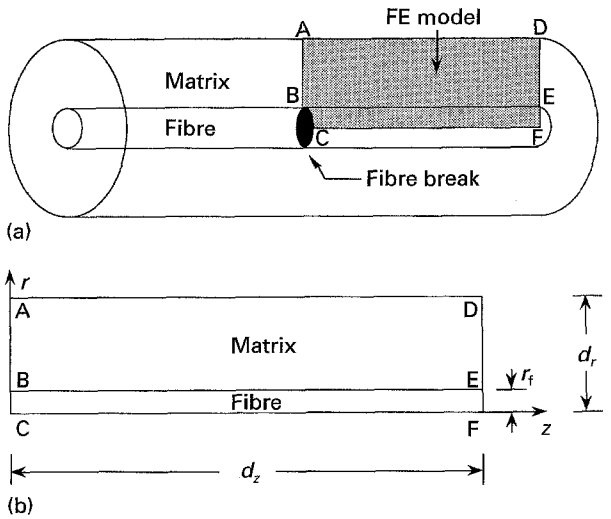

Figure 1 (a) Single-fibre composite. (b) Axisymmetric finite element model.

The baseline materials are chosen to be a stiff or soft epoxy matrix containing an S-glass or E-glass fibre. The following material properties are used [3] : stiff epoxy: $E = 2.9$ GPa, $\nu = 0.35$, $\rho = 1.23\ g\,cm^{-3}$; soft epoxy: $E = 1.6$ GPa, $\nu = 0.35$, $\rho = 1.23\ g\,cm^{-3}$; S-glass: $E = 86.9$ GPa, $\nu = 0.22$, $\rho = 2.46\ g\,cm^{-3}$, $r_f = 5\ \mu m$; E-glass: $E = 72.0$ GPa, $\nu = 0.22$, $\rho = 2.46\ g\,cm^{-3}$, $r_f = 6.5\ \mu m$.

The axial and shear stresses (σ_{zz} and σ_{rz}) at the crack tip (point B) as a function of time following fibre breakage are shown in Figs 2 and 3, respectively, for an S-glass fibre in an epoxy A matrix. For comparison, the values from a static analysis of the model with a broken fibre are shown. The dynamic stresses start at the static values for an unbroken fibre, increase rapidly and obtain their maximum values, then oscillate around the static values for a broken fibre. This behaviour is expected, because no damping is included in the analysis. The maximum dynamic stresses at the crack tip and corresponding times are given in Table I. The dynamic amplification factor (DAF) is defined as the ratio of the maximum dynamic stress divided by the static stress. From Table I it is seen that the DAF and times are approximately the same for all four components of stress.

The spatial distributions of the axial and shear stresses along the fibre–matrix interface (BE in Fig. 1) are shown in Figs 4 and 5, respectively. The spatial distributions of these stresses along the matrix (BA in

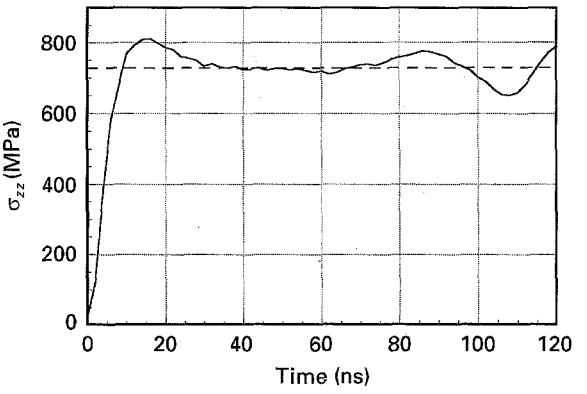

Figure 2 Single-fibre composite: axial stress versus time at the crack tip (point B in Fig. 1) following fibre breakage: (—) dynamic, (– – –) static.

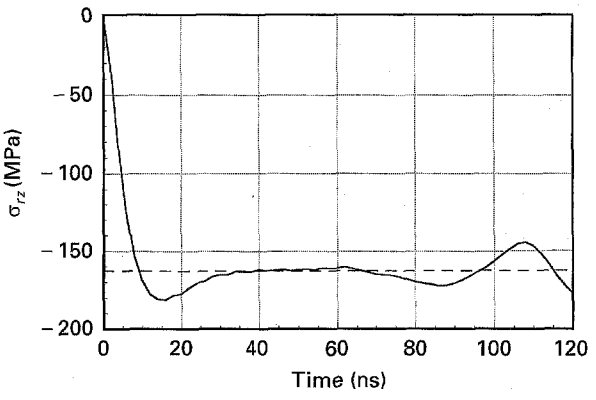

Figure 3 Single-fibre composite: shear stress versus time at the crack tip (point B in Fig. 1) following fibre breakage: (—) dynamic, (– – –) static.

TABLE I Dynamic results for stiff epoxy/S-glass

Stress	Static (MPa)	Dynamic (MPa)	DAF	Time (ns)
σ_{zz}	727.6	812.7	1.117	15
σ_{rz}	162.8	181.6	1.115	14
$\sigma_{\theta\theta}$	257.0	288.7	1.123	15
σ_{rr}	134.4	153.4	1.141	15

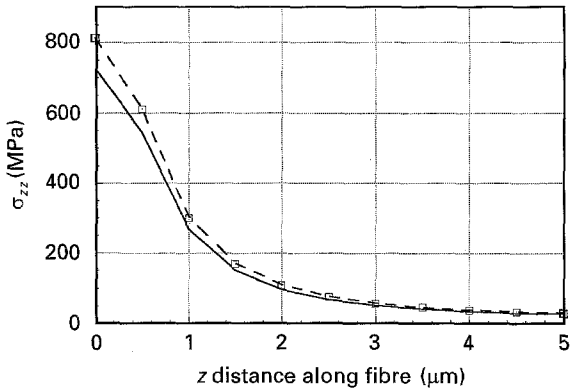

Figure 4 Single-fibre composite: axial stress along the fibre–matrix interface (side BE in Fig. 1) : (—) static, (□) DAF* static, (– – –) maximum dynamic.

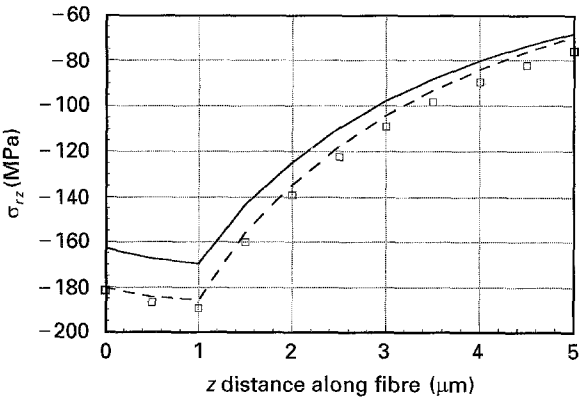

Figure 5 Single-fibre composite: shear stress along the fibre–matrix interface (side BE in Fig. 1) : (—) static, (□) DAF* static, (– – –) maximum dynamic.

Fig. 1) are shown in Figs 6 and 7. In these figures, the maximum dynamic stresses, static stresses with a fibre break, and the static stresses scaled by the DAF are shown. It is seen that the spatial distribution of the static and dynamic stresses are similar, and if the static stresses are scaled by the DAF, they agree closely with the dynamic stresses. Therefore, if the static stresses are known, the dynamic effects can be characterized by a DAF.

The range of values for the DAF was evaluated for S-glass and E-glass fibres embedded in different epoxy matrices. For this evaluation, only the value of Young's modulus of the matrix, E_m, was changed. Tables II and III summarize the matrix modulus values and give results for the DAF and time for the maximum stress for S-glass and E-glass fibres, respectively. The ratio of the longitudinal wave speeds for the fibre and matrix (C_f/C_m) is also given. The DAF

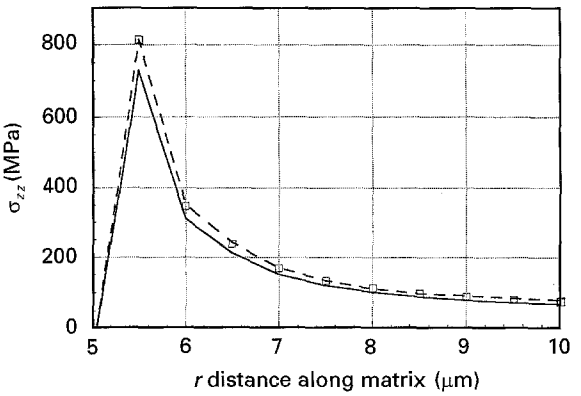

Figure 6 Single-fibre composite: axial stress along the matrix (side BA in Fig. 1): (—) static, (□) DAF* static, (– – –) maximum dynamic.

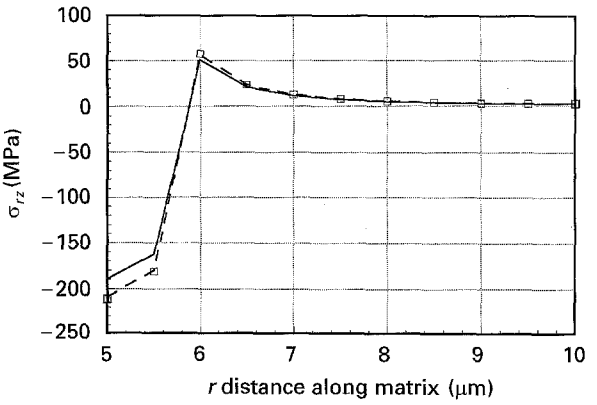

Figure 7 Single-fibre composite: shear stress along the matrix (side BA in Fig. 1) : (—) static, (□) DAF* static, (– – –) maximum dynamic.

TABLE II Dynamic results for S-glass

Case	E_m (GPa)	C_f/C_m	DAF	Time (ns)
1	2.90	3.87	1.117	15
2	2.15	4.50	1.094	18
3	1.60	5.21	1.077	22
4	1.03	6.50	1.047	30
5	0.68	8.00	1.024	46

TABLE III Dynamic results for E-glass

Case	E_m (GPa)	C_f/C_m	DAF	Time (ns)
1	2.90	3.52	1.128	15
2	2.15	4.10	1.110	16
3	1.60	4.74	1.088	20
4	1.03	5.92	1.057	27
5	0.67	7.28	1.034	40

and time for maximum stress are plotted versus wave speed ratio in Figs 8 and 9, respectively. The results for S-glass and E-glass overlap, suggesting that the wave speed ratio can be used to characterize these results. The DAF ranges from 1.024–1.128 for glass fibres embedded in these epoxy matrices. The axial stress at

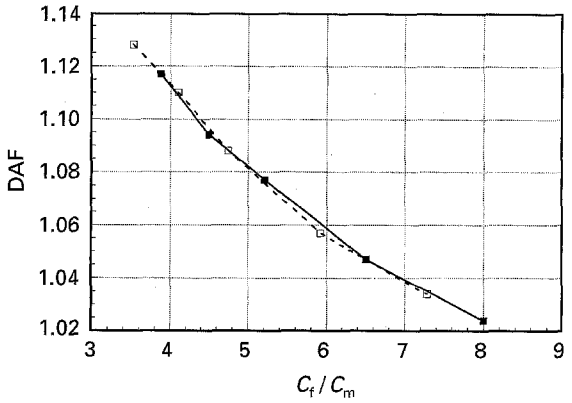

Figure 8 Single-fibre composite: dynamic amplification factor versus ratio of wave speeds. (–■–) S-glass, (– –□– –) E-glass.

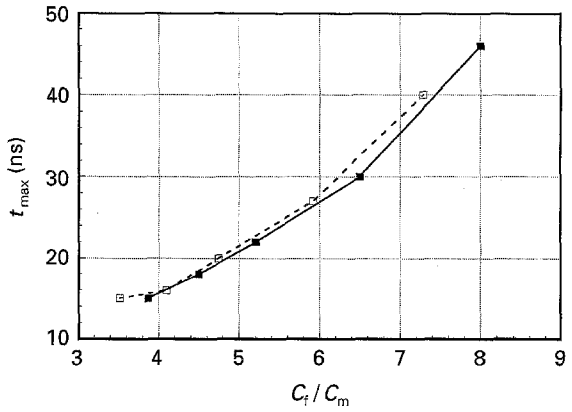

Figure 9 Single-fibre composite: time for maximum stress versus the ratio of wave speeds. (–■–) S-glass, (– –□– –) E-glass.

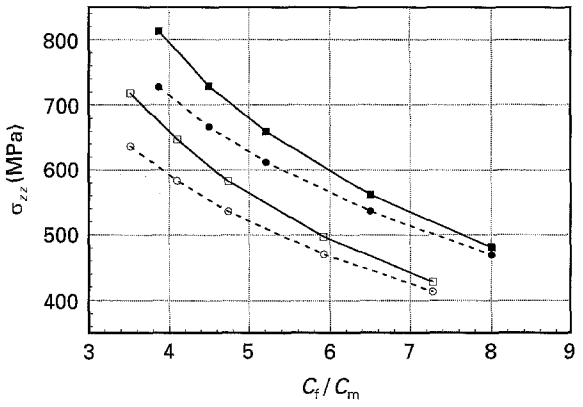

Figure 10 Single-fibre composite: axial stress at the crack tip versus the ratio of wave speeds. S-glass: (–■–) dynamic, (– –●– –) static. E-glass: (–□–) dynamic, (– –○– –) static.

the crack tip is plotted versus wave speed ratio in Fig. 10. It is seen that the largest DAF occurs for the smallest wave speed ratio which corresponds to the case with the highest static stress. Therefore, the dynamic effects are most significant for this case.

3. Multiple-fibre composite

In this section, the dynamic effects of fibre breakage are examined for a two-dimensional (plane strain) composite material containing multiple fibres, as shown in Fig. 11a. The finite element model (ABCD) is

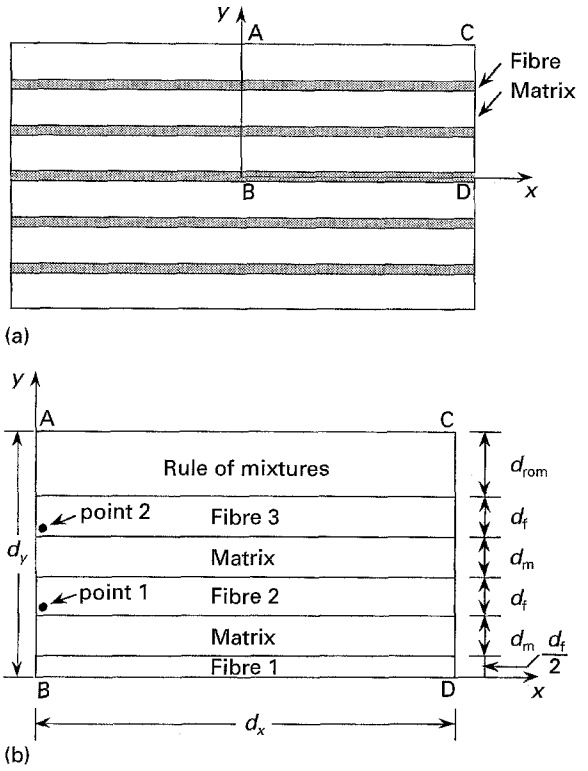

Figure 11 (a) Multiple-fibre composite. (b) Plane strain finite element model.

shown in Fig. 11b. In this model, three fibres and two matrix regions are explicitly modelled and the properties of the composite obtained from a rule of mixtures are used in the outer region. The overall dimensions are, again, chosen sufficiently large to ensure that the waves caused by fibre breakage do not impinge a boundary ($d_x = 600$ μm, $d_y = 103$ μm) . The boundary conditions for this model are similar to those described for the single-fibre model. Approximately 10 800 plane strain elements were used in the finite element model.

For the case considered, the spacing of the fibres is equal to the fibre diameter ($d_m = d_f = 14$ μm) which gives a fibre volume fraction of $v_f = 0.556$. A stiff epoxy matrix and E-glass fibres are used. The following properties for the composite region (d_{rom}) are obtained using the rule of mixtures: $E_{11} = 41.3$ GPa, $E_{22} = 10.8$ GPa, $G_{12} = 3.67$ GPa, $G_{31} = 3.67$ GPa, $G_{23} = 3.60$ GPa, $\nu_{12} = 0.278$, $\nu_{31} = 0.0727$, $\nu_{23} = 0.5$.

The stresses at points 1 and 2 in fibres 2 and 3, shown in Fig. 11b, were monitored over time for two cases. These points are slightly inside the lower left corner of the fibres. In the first case (dynamic 1), only fibre 1 is broken. In the second case (dynamic 2), fibre 2 is also broken after reaching its maximum dynamic stress values caused by the breaking of fibre 1. Both fibres are broken at edge AB by releasing the displacement boundary condition on the fibre along that edge. The corresponding static analyses (static 1 and 2) were also performed for comparison. All cases correspond to an initial strain of 1%.

The axial stress (σ_{xx}) at points 1 and 2 versus time following fibre 1 breakage are shown in Figs 12 and 13, respectively, for both cases. For case 1, the axial stress at point 1 increases from the static value with no

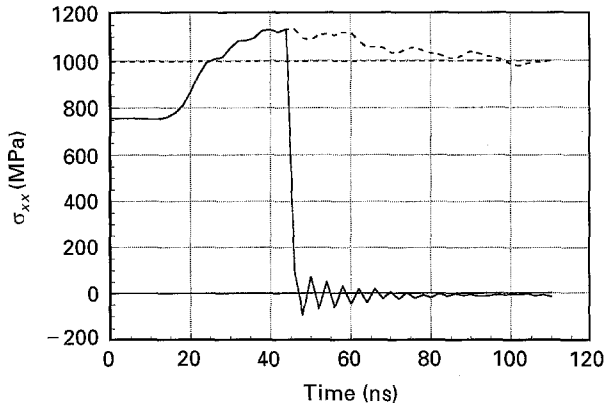

Figure 12 Multiple-fibre composite: axial stress at point 1 of Fig. 11 versus time for case 1 (only fibre 1 is broken) and case 2 (fibre 2 is also broken after reaching its maximum dynamic stress values caused by the breaking of fibre 1). (– – –) Static 1, (—) static 2, (– – –) dynamic 1, (—) dynamic 2.

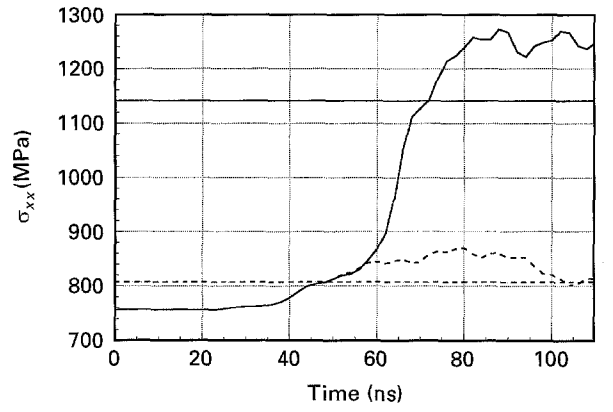

Figure 13 Multiple-fibre composite: axial stress at point 2 of Fig. 11 versus time for case 1 (only fibre 1 is broken) and case 2 (fibre 2 is also broken after reaching its maximum dynamic stress values caused by the breaking of fibre 1). (– – –) Static 1, (—) static 2, (– – –) dynamic 1, (—) dynamic 2.

fibre breakage to its maximum value at $t = 44$ ns, as seen in Fig. 12. In fibre 3 at point 2, the maximum stress due to breakage of fibre 1 is not reached until a later time ($t = 80$ ns) because point 2 is further from the break, as seen in Fig. 13. For case 2, it is assumed that fibre 2 breaks when it reaches its maximum stress at $t = 44$ ns. When fibre 2 breaks, the stress at point 1 drops to approximately zero, as seen in Fig. 12. The stress is then transferred dynamically to fibre 3. As seen in Fig. 13, the stress in fibre 3 increases dramatically after fibre 2 breaks and reaches a maximum at $t = 88$ ns. Numerical results are given in Table IV. The dynamic effects associated with breakage of fibre 1 increase the stress at fibre 2 by a factor of 1.135 over the corresponding static value. The dynamic effects associated with breakage of fibre 2 increase the stress at fibre 3 by a factor of 1.116 over the corresponding static value. The axial stress along fibres 2 and 3 at their maximum dynamic stress state ($t = 44$ and 88 ns, respectively), the corresponding static values, and the static values scaled by the DAF are shown in Figs 14 and 15, respectively. From these plots, it is seen that the spatial distribution of the dynamic stress differs significantly from the corresponding static distribution.

TABLE IV Results for multiple-fibre composite

	Static(MPa)		Dynamic(MPa)		DAF	
	1	2	$t = 44$ ns	$t = 88$ ns	1	2
σ_{xx} at point 1	996.2		1130.7		1.135	
σ_{xx} at point 2		1140.3		1272.4		1.116

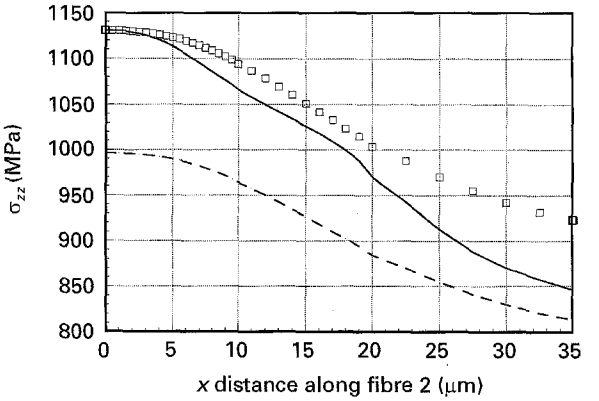

Figure 14 Multiple fibre composite: axial stress along fibre 2 for case 1 (only fibre 1 is broken). (– – –) Static 1; (□) DAF* static; (—) dynamic, $t = 44$ ns.

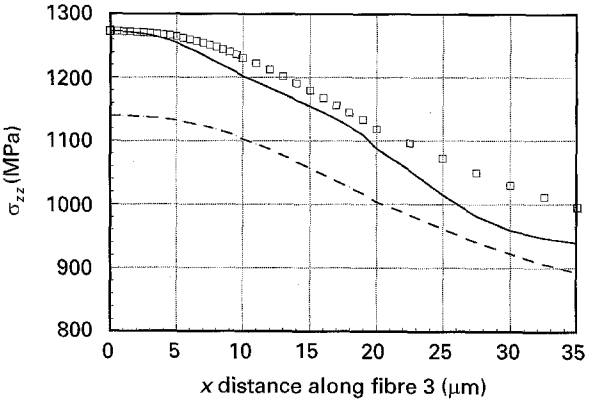

Figure 15 Multiple fibre composite: axial stress along fibre 3 for case 2 (fibre 2 is also broken after reaching its maximum dynamic stress values caused by the breaking of fibre 1). (– – –) Static 2; (□) DAF* static; (—) dynamic, $t = 88$ ns.

In a previous analysis on this same microcomposite system, the static stresses and strains on matrix and fibres adjacent to a single filament break were simulated and then used to calculate the probability of fracture of the adjacent fibre as a function of the distance along its axis [4]. Because the extent of interphase and/or matrix cracking at the initial fibre break influences the magnitude of stresses on adjacent fibres, the simulations were carried out as a function of the extent of precracking at the original fibre break.

To calculate the probability of fracture of the adjacent fibre, it was necessary to define a fibre strength distribution as a function of fibre length. Fibre strength distributions for various E-glass fibres used in the authors' laboratory have been reported in other publications [5–8]. A representative Weibull function for the length of E-glass fibres used in the LFEM

analyses is

$$G(\sigma) = 1 - \exp\left[- L\left(\frac{\sigma}{\beta}\right)^{\alpha}\right] \qquad (1)$$

where $G(\sigma)$ is the cumulative probability of failure, $L = 1.210$ mm, $\alpha = 2.78$ and $\beta = 1989$ MPa mm$^{1/\alpha}$.

In the simulation of fracture of a single filament, the fibre is broken at an axial stress of σ_p. The adjacent fibres having been loaded to the same stress, but not broken, have been mechanically proof tested to σ_p. Because it is clear that they have zero probability of failing below this level of stress, their statistical strength properties will be described by a truncated cumulative distribution function. Assuming that the surviving fibres were unaffected by the proof test, one can show that the appropriate form of a truncated Weibull distribution function, $G_p(\sigma)$, is related to the original distribution, $G(\sigma)$, by the following expression [9]

$$G_p(\sigma) = \frac{G(\sigma) - G(\sigma_p)}{1 - G(\sigma_p)} \qquad (\sigma \geq \sigma_p) \qquad (2)$$

$$G_p(\sigma) = 0 \qquad (\sigma < \sigma_p) \qquad (3)$$

where σ_p is the proof test stress. By calculating the stress concentrations on adjacent fibres caused by a fibre break, one can then use the truncated distribution to calculate the probability of failure at a point on an adjacent fibre.

Axial stress concentration factors along the near side of fibres 2 and 3 at their maximum dynamic stress states ($t = 44$ and 88 ns, respectively), along with the corresponding static values, are shown in Figs 16 and 17, respectively. The results are scaled to a strain of 2.11% at which point the central filament is fractured at approximately its average strength of 1600 MPa (i.e. $G(\sigma) = 0.481$). The choice of boundary condition upon release of the fibre mesh nodes imposes an interfacial crack equivalent to one mesh unit at the broken fibre end. The corresponding probabilities of failure as a function of the distance from the broken fibre end are shown in Figs 18 and 19. From Fig. 18 one can see that at constant strain the probability of fracture of the nearest adjacent fibre at point 1 increases to G_p (2106 MPa) = 0.53 based on the maximum level of static stress and G_p (2391 MPa) = 0.74 based on the maximum level of dynamic stress. From Fig. 19 one can see that if the nearest adjacent fibre fractures at the peak of its dynamic wave (i.e. at 44 ns), the probability of having a third fibre break at 88 ns, in the same plane as the other two, has increased to G_p (2411 MPa) = 0.75 based on the maximum level of

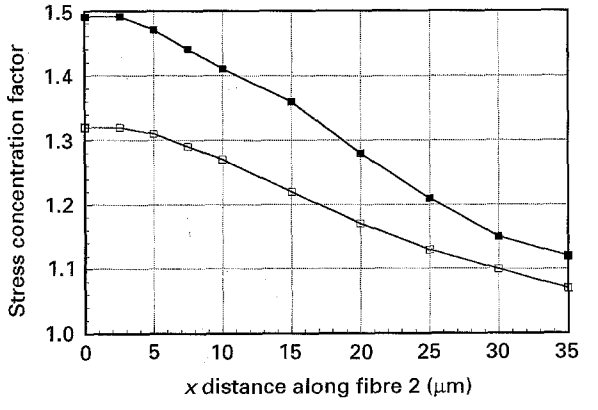

Figure 16 Multiple-fibre composite: axial stress concentration factor along fibre 2 for case 1 (only fibre 1 is broken). (–□–) Static stress/1600 MPa; (–■–) dynamic stress at 44 ns/1600 MPa.

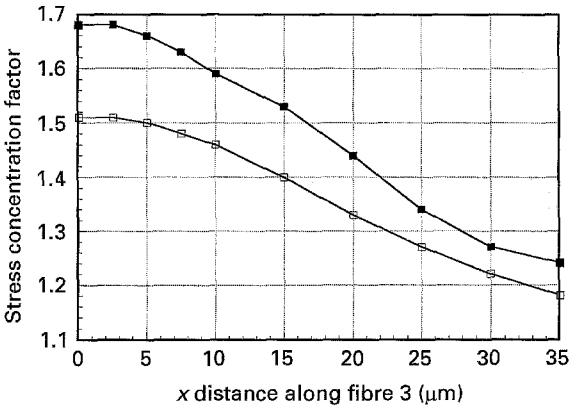

Figure 17 Multiple-fibre composite: axial stress concentration factor along fibre 3 for case 2 (fibre 2 is also broken after reaching its maximum dynamic stress values caused by the breaking of fibre 1). (–□–) Static stress/1600 MPa; (–■–) dynamic stress at 88 ns/1600 MPa.

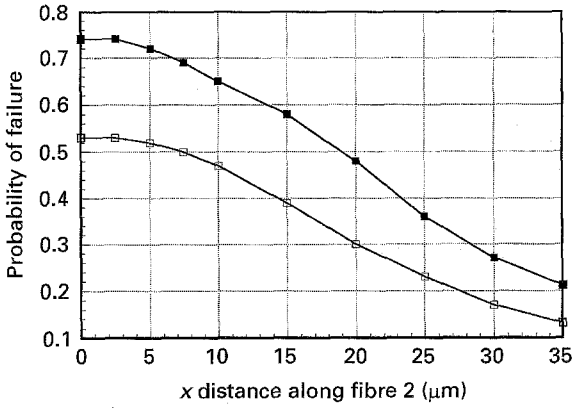

Figure 18 Multiple-fibre composite: probability of fibre failure along fibre 2 for case 1 (only fibre 1 is broken). (–□–) Static, (–■–) dynamic at 44 ns.

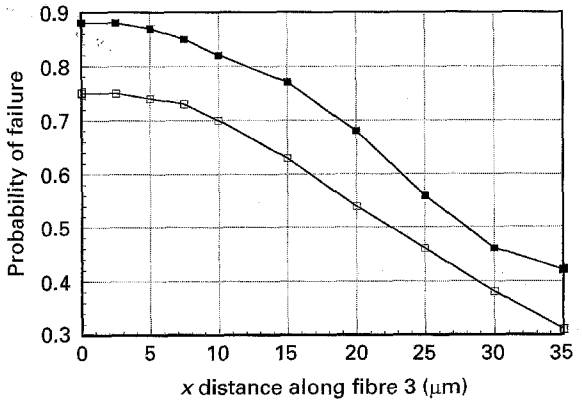

Figure 19 Multiple fibre composite: probability of fibre failure along fibre 3 for case 2 (fibre 2 is also broken after reaching its maximum dynamic stress values caused by the breaking of fibre 1). (–□–) Static, (–■–) dynamic at 88 ns.

static stress and to G_p (2690 MPa) = 0.88 based on the maximum level of dynamic stress. Because the dynamic processes are occurring at longitudinal wave speeds, it is expected that both the glassy polymer matrices and the glass fibres will experience linear elastic behaviour during this 100 ns period. Furthermore, subsequent failures of adjacent fibres should continue with an increasing probability until various damping mechanisms put an end to the damage. Experimentally, it is observed that in the microcomposites the subsequent failures occur almost immediately, and, when the fibre spacing is less than three to four fibre diameters, in a coordinated planar pattern. Thus, the computer simulation appears to describe accurately the experimental results.

4. Conclusion

Dynamic effects associated with fibre breakage in single- and multiple-fibre microcomposites have been investigated using the linear elastic finite element method. The dynamic stresses occurring in both cases are shown to be significantly different from the calculated static stresses and, consequently, have an important effect on the prediction of subsequent fibre failure in the composite. For single-fibre composites, the dynamic stresses generated by a single filament fracture increase rapidly to a maximum and then decrease and oscillate around the calculated values of the static stresses. The amplification of all four components of the stress is approximately equal at a specific point along the fibre/matrix interface and thus the dynamic stress state can be characterized by a single dynamic amplification factor (DAF). For the single-fibre glass/epoxy microcomposites investigated, the DAF ranges from approximately 1.02–1.15 and is independent of the position along the fibre/matrix interface. The time to reach maximum dynamic stress adjacent to the crack tip ranges from approximately 15–50 ns. Both quantities decrease monotonically with the ratio of the longitudinal wave speeds in the fibre and matrix, respectively, which appears to be the primary variable characterizing the dynamic process. For the multiple fibre composites with 55.6% by volume of fibres, similar values for the DAF are obtained. Although a single value of the DAF can be used to describe the spatial distribution of the four components of the dynamic stress at a specific point in an adjacent fibre, its value varies with distance along the fibre axis. Thus, the spatial distribution of the dynamic stresses differs significantly from the corresponding static distribution. Using a truncated Weibull function to relate the probability of failure of adjacent fibres to the maximum dynamic stress experienced because of a fibre break, one can show that the dynamic processes can substantially increase the probability of failure and can potentially lead to a higher probability of a cascading effect that will result in a co-ordinated pattern of fibre fracture in the microcomposite. The results of these simulations are consistent with experimental observations reported in the literature.

References

1. K. D. JONES and A. T. DIBENEDETTO, *Compos. Sci. Technol.* **51** (1994) 53.
2. P. W. J. VAN DEN HEUVEL, Y. J. W. VAN DER BRUGGER and T. PEIJS, *Adv. Compos. Lett.* **3** (6) (1994) 197.
3. A. PEGORETTI, M. L. ACCORSI and A. T. DIBENEDETTO, *J. Mater. Sci.* **31** (1996) 4181.
4. K. D. JONES and A. T. DIBENEDETTO, "IPCM 95", Eindhoven, September 1995, *J. Compos.*, in press.
5. A. DIANSELMO, M. L. ACCORSI and A. T. DIBENEDETTO, *Compos. Sci. Technol.* **44** (1992) 215.
6. K. D. JONES and A. T. DIBENEDETTO in "Proceedings of the 3rd International Conference on Deformation and Fracture of Composites", March 1995, pp. 86–95.
7. W. A. FRASER, F. H. ANCKER, A. T. DIBENEDETTO and B. ELBERLI, *Polym. Compos.* **4** (1983) 238.
8. A. T. DIBENEDETTO and P. J. LEX, *Polym. Eng. Sci.* **29**(8) (1989) 543.
9. W. WEIBULL, *J. Appl. Mech. (ASME)* **18** (1951) 293.

Received 3 January
and accepted 18 March 1996